Remote Sens. **2012**, *4*, 354-376; doi:10.3390/rs4020354

OPEN ACCESS

Remote Sensing

ISSN 2072-4292

www.mdpi.com/journal/remotesensing

Article

Inter-Sensor Comparison between THEOS and Landsat 5 TM Data in a Study of Two Crops Related to Biofuel in Thailand

Naruemon Phongaksorn [1], Nitin K. Tripathi [1,*], Sivanappan Kumar [2] and Peeyush Soni [3]

[1] Remote Sensing and Geographic Information Systems, School of Engineering and Technology, Asian Institute of Technology, Thailand; E-Mail: st106182@ait.ac.th

[2] Energy, School of Environment, Resources and Development, Asian Institute of Technology, Thailand; E-Mail: kumar@ait.ac.th

[3] Agricultural Systems and Engineering, School of Environment, Resources and Development, Asian Institute of Technology, Thailand; E-Mail: soni@ait.ac.th

* Author to whom correspondence should be addressed; E-Mail: nitinkt@ait.ac.th; Tel.: +66-2-524-6392; Fax: +66-2-524-5597.

Received: 8 December 2011; in revised form: 16 January 2012 / Accepted: 19 January 2012 / Published: 1 February 2012

Abstract: Knowledge of the spatial distribution of biofuel crops is an important criterion to determine the sustainability of biofuel energy production. Remotely sensed image analysis is a proven and effective tool for describing the spatial distribution of crops using vegetation characteristics. Increases in the number of options and availability of satellite sensors have expanded the horizon of choices of imagery sources for appropriate image acquisitions. The Thailand Earth Observation System (THEOS) satellite is one of the newest satellite sensors. The growing number of satellite sensors warrants their comparative evaluation and the standardization of data obtained from various sensors. This study conducted an inter-sensor comparison of the visible/near-infrared surface reflectance and Normalized Difference Vegetation Index (NDVI) data collected from the Landsat 5 Thematic Mapper (TM) and THEOS. The surface reflectance and the derived NDVI of the sensors were randomly obtained for two biofuel crops, namely, cassava and sugarcane. These crops had low values of visible surface reflectance, which were not significantly ($p < 0.05$) different. In contrast, the crops had high values of near-infrared surface reflectance that differed significantly ($p > 0.05$) between the crops. Strong linear relationships between the remote sensing products for the examined sensors were obtained for both cassava and sugarcane. The regression models that were developed can be used to compute the NDVI for THEOS using those determined from Landsat 5 TM and *vice versa* for the given

biofuel crops.

Keywords: biofuel crops; THEOS; Landsat 5 TM; radiometric calibration; 6S model; surface reflectance; NDVI; spatial accuracy assessment

1. Introduction

Knowledge of the spatial information for biofuel crops, which includes the geographical location and spatial distribution, are important criteria for determining the sustainability of renewable energy production at different spatial scales [1–3]. Remote sensing image analysis has become an effective tool for describing the spatial distributions of vegetation characteristics, including crop types and their quality, quantity, and geographic distribution over the last 30 years, from local to regional and global spatial scales [4,5]. Satellite sensors have a wide range of temporal frequency and spatial resolution, from high resolution and narrow swath width to lower resolution and larger swath width. The higher resolution systems can provide the spatial details required, but their revisiting periods are somewhat longer, particularly when data acquisition is limited by cloud cover. As a consequence, the application of multiple satellite sensors for data collection is of great interest among user communities to combine data from various observing systems to fill in gaps in observations. It is also valuable to establish a relationship between the high-resolution measurements of vegetation and more frequent measurements of lower resolution systems [5–10]. The THEOS satellite can acquire both high-resolution panchromatic and large-swath multispectral data. It can also be used for frequent revisiting of areas for natural resource and environment monitoring, which has numerous applications, such as in cartography, land use analyses, agricultural monitoring, forestry management, coastal zone monitoring, and flood risk management. Launched in 2008, THEOS, is one of the newest satellite sensors and Thailand's first Earth resource observation satellite [11].

The increasing number of satellite sensors necessitates cross-sensor standardization of data [5,12]. There are several techniques for this evaluation, which include radiometric, spatial, and temporal calibration [7,9]. Numerous studies have been done to compare the relative performances of sensors. Hill *et al.* [6] calibrated the radiometric relationship between Landsat 5 TM and field reflectance and also compared the radiometric accuracy of Satellite Pour l'Observation de la Terre High Resolution Visible (SPOT HRV) and Landsat 5 TM. The results of their calibration indicate that the visible and near-infrared wavelengths are highly related. Moreover, a linear relationship was also found between both systems for the NDVI information on agricultural, forest, and non-vegetated cover types in France. Steven *et al.* [8] studied the effects of the sensor spectral characteristics of NDVI on sugar beet (*Beta vulgaris,* L.), and showed a strong linear relationships, while establishing conversion factors for the Advanced Very High Resolution Radiometer (AVHRR), Advanced Along-Track Scanning Radiometer (ATSR-2), Landsat (Landsat 4 Multispectral scanner: MSS, Landsat 5 TM, and Landsat 7 Enhance Thematic Mapper Plus: ETM+), SPOT-2 and SPOT-4 HRV, Indian Resource Satellite (IRS), IKONOS, Sea-viewing Wide Field-of-view Sensor (SEAWIFS), Multi-angle Imaging SpectroRadiometer (MISR), MODerate Resolution Imaging Spectroradiometer (MODIS), POLarization and Directionality of the Earth's Reflectance (POLDER), QuickBird, and MEdium Resolution Imaging

Spectrometer (MERIS) sensors. Thenkabail [9] compared the visible and near-infrared wavelengths of IKONOS and Landsat 7 ETM+ and conducted an NDVI inter-sensor regression analysis for three distinct eco-regions of African rainforests and savannas. Their results indicate that the IKONOS visible and near-infrared wavelengths have a high degree of correlation with those from ETM+. Inter-sensor model equations relating IKONOS NDVI with ETM+ NDVI were also determined for multiple sensors over time. Miura *et al.* [10] compared the products from ASTER and MODIS sensors for the visible/near-infrared surface reflectance and spectral vegetation indices (VIs), namely, NDVI and the Enhanced Vegetation Index (EVI). The results show that the surface reflectance products and NDVI of the two sensors compared well at a global scale.

Though several studies are available for a variety of satellite sensors that have been applied to crop studies, there is no comparative work for the surface reflectance and NDVI between THEOS and Landsat 5 TM, especially for cassava and sugarcane [5–10,13–16]. Cassava and sugarcane are agricultural crops that are increasingly used for biofuels in Thailand [17]. The Landsat 5 TM sensor was selected for comparison because the location and bandwidth of the visible and near-infrared channels are similar to those of THEOS followed advice of Hill *et al*. [6] and it is one of the most frequently used sensors for radiometric calibration [6,8] and terrestrial applications [18–21]. In addition, Landsat 5 TM was calibrated in 2003 and was further revised in 2007, based on the detectors' responses to pseudo-invariant desert sites and cross-calibration with ETM+ [22]. The important remote sensing products for the analysis of radiometric accuracy of a sensor are the surface reflectance and Normalized Difference Vegetation Index (NDVI) [5–10]. Thus, this study was conducted with four main objectives: (a) to investigate the spectral characteristics of two biofuel crops (cassava and sugarcane); (b) to compare the surface reflectance and NDVI between Landsat 5 TM and THEOS; (c) to develop NDVI regression models between THEOS and Landsat 5 TM for multiple satellite sensors; and (d) to perform classification and spatial accuracy assessment. The results are expected to provide an alternate approach for the frequent monitoring of biofuel crops using the THEOS and Landsat 5 TM satellites. The study was conducted using data from two provinces of Thailand representing a wide range of cassava and sugarcane cultivations.

2. Study Areas

Two provinces of Thailand, Nakhon Ratchasima (14°58′20″N and 102°6′0″E) and Suphanburi (14°28′12″N and 100°7′48″E), with approximately 1,500–2,000 ha that are planted with cassava and sugarcane, comprised the study area (Figure 1). The surface reflectance and NDVI of cassava were studied in Nakhon Ratchasima Province, whereas Suphanburi Province was considered for sugarcane. A total of sixty biofuel crop sites were sampled in Market Year (MY) 2008/09: thirty samples for cassava and thirty samples for sugarcane as depicted in Figure 1.

3. Materials and Methods

3.1. Satellite Images

One THEOS and one Landsat 5 TM image were acquired for the same acquisition period in MY 2008/09 (Figure 2). The acquisition dates and characteristics of the images are listed in Tables 1 and 2.

Figure 1. Study areas and locations of sample fields marked on a THEOS image. (**a**) Cassava site in Nakhon Ratchasima Province. (**b**) Sugarcane site in Suphanburi Province.

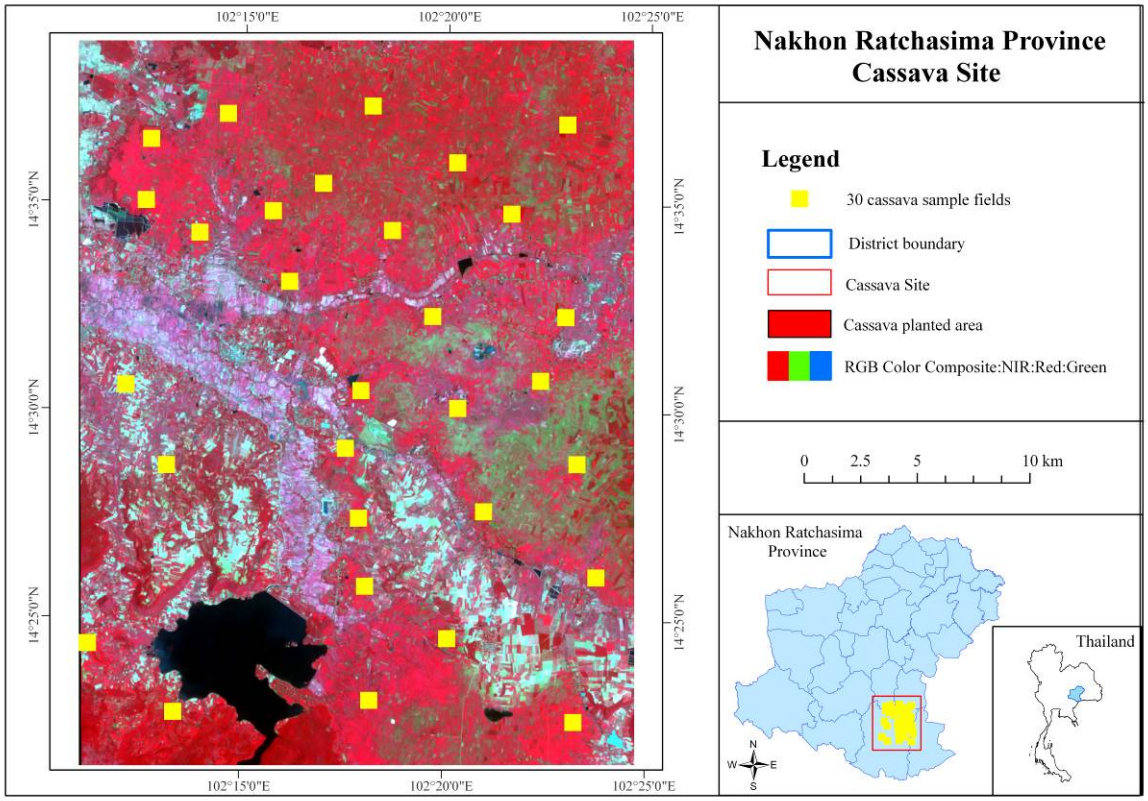

(**a**)

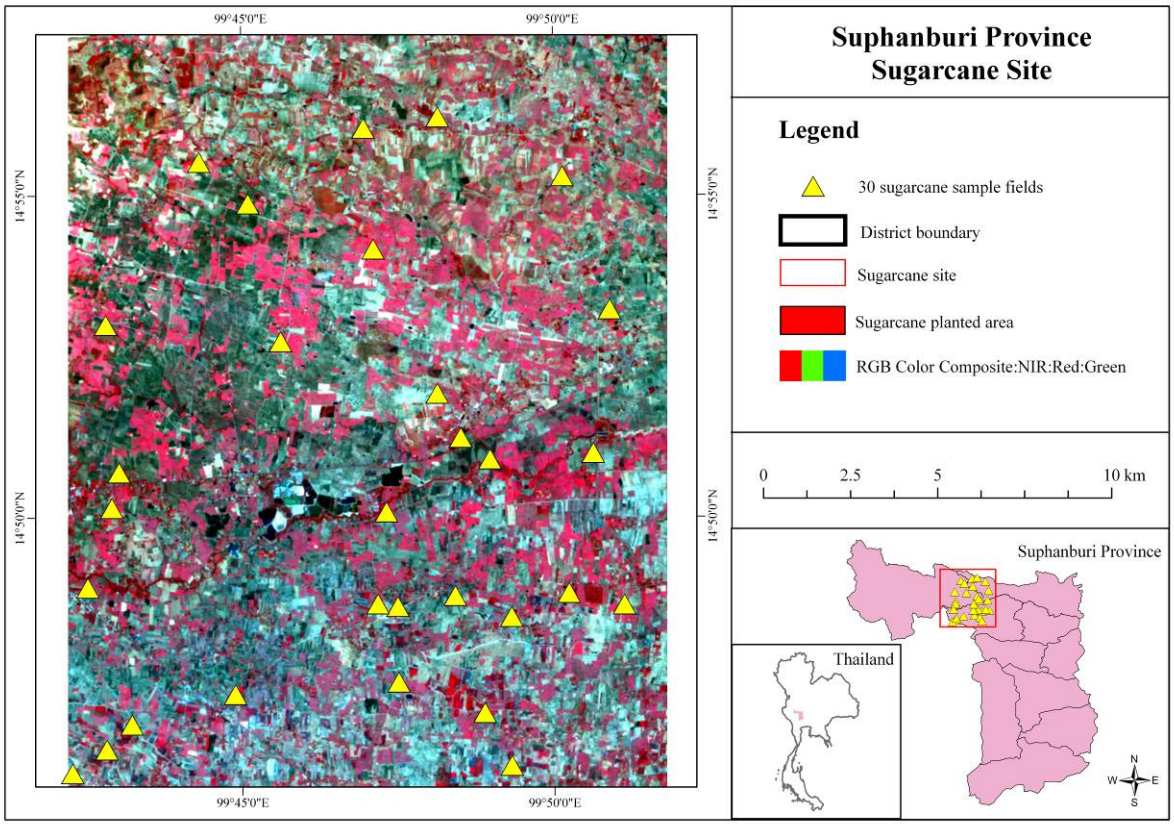

(**b**)

Figure 2. Multispectral images from THEOS and Landsat 5 TM for the study area: (**a**) THEOS for cassava. (**b**) Landsat 5 TM for cassava. (**c**) THEOS for sugarcane. (**d**) Landsat 5 TM for sugarcane.

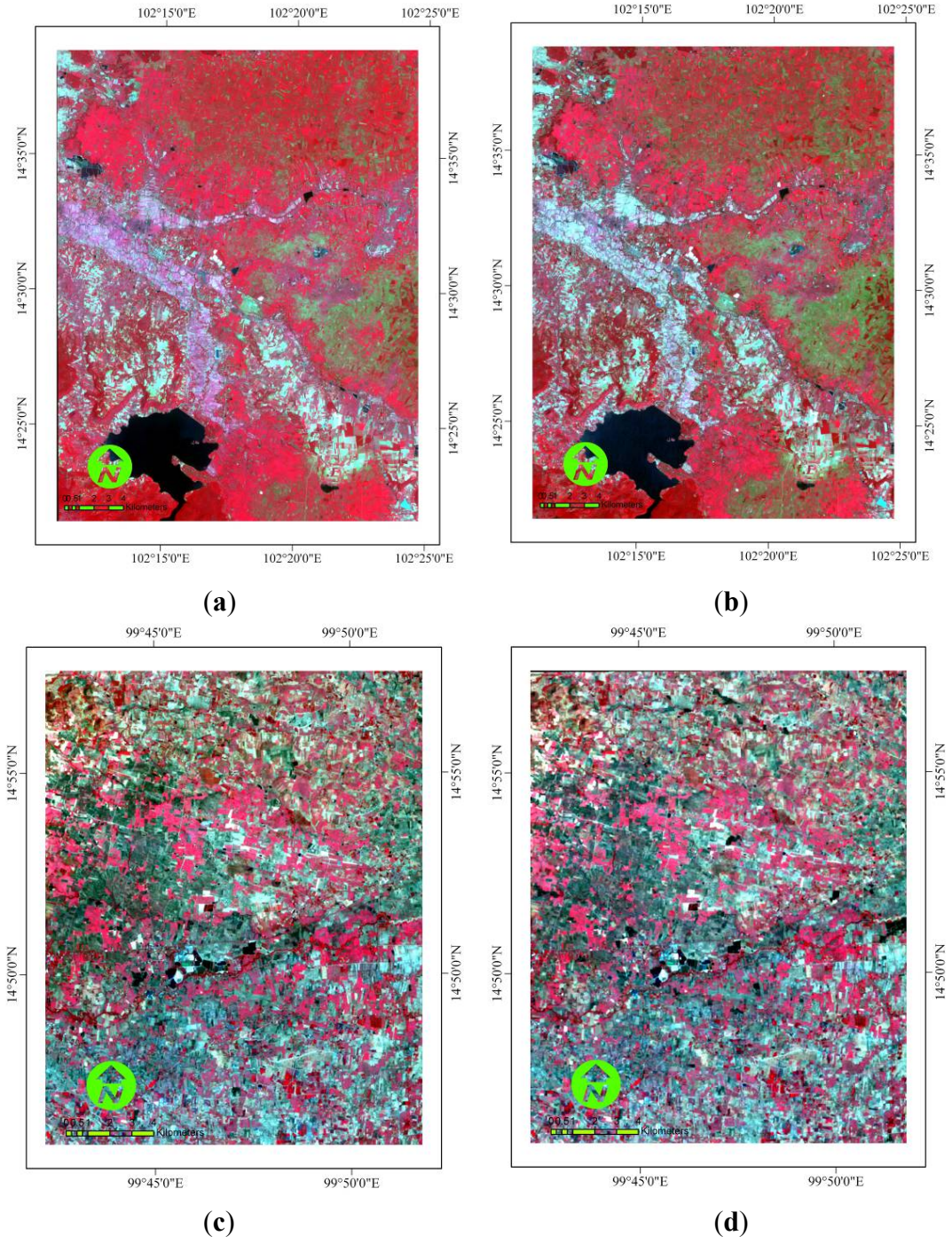

Table 1. Acquisition of THEOS and Landsat 5 TM images for the study area.

Study Area	Biofuel Crop	Satellites	Date of Acquisition (dd/mm/yy)
Nakhon Ratchasima Province	Cassava	THEOS	29/11/08
		Landsat 5 TM	11/12/08
Suphanburi Province	Sugarcane	THEOS	9 /02/09
		Landsat 5 TM	11/02/09

Table 2. Sensor characteristics of four multispectral bands of THEOS and Landsat 5 TM used in the study.

Sensor	* Spatial Resolution (m)	Band Number Abbreviation	* Spectral Range (nm)	*Center Wavelength (nm)
THEOS	15	TH1	450–520	485
		TH2	530–600	565
		TH3	620–690	655
		TH4	770–900	835
Landsat 5 TM	30	TM1	450–520	485
		TM2	520–600	560
		TM3	630–690	660
		TM4	760–900	830

* THEOS: Geo-Informatics and Space Technology Development Agency (Public Organization) (GISTDA), Thailand; Landsat 5 TM: National Aeronautics and Space Administration (NASA), USA.

3.2. Satellite Data Processing and Analysis

Images obtained from the THEOS and Landsat 5 TM sensors were corrected geometrically and atmospherically. Geometric correction dealt with the spatial distortions, whereas atmospheric correction removed the influences of scattering and the absorption of atmospheric molecules and aerosols on an object's reflectance.

In the geometric correction for inter-sensor comparison, the THEOS image was spatially re-sampled at a 15 m spatial resolution using the nearest neighborhood procedure and then set to the WGS-84 projection. Ground Control Points (GCPs) were selected on the image and on the topography map. Image rectification was based on a first-order polynomial transformation with an acceptable root mean square error (RMSE) of about 0.004. Then, the geometrically corrected THEOS image was used as a reference for the geometric correction of the Landsat 5 TM image. The Landsat 5 TM images were then spatially re-sampled at the THEOS spatial resolution. The same GCPs were selected on the THEOS and Landsat 5 TM images. Image rectification was based on a first-order polynomial transformation with an acceptable RMSE of about 0.004 [5]. Following geometric correction, the satellite images were processed using low pass filtering with a 3 × 3 kernel to solve for any discrepancies in the positions of sampling points from the Global Positioning System (GPS). The error from GPS measurements ranged from less than a meter to around 30 m and was adjusted accordingly [23].

The atmospheric correction consisted of three steps. First, the atmospheric correction converted the digital numbers (DN) into a spectral radiance at a sensor's aperture (L_λ) using the sensor's gains. The gains of THEOS and Landsat 5 TM were given on their image header files and the at-sensor spectral radiances of THEOS for each band were calculated using the following equation.

$$L^i{}_{\lambda_{THEOS}} = \frac{DN^i}{G^i} \tag{1}$$

where $L^i{}_{\lambda_{THEOS}}$ is the spectral radiance at the sensor's aperture of THEOS for band i ($Wm^{-2}\cdot sr^{-1}\cdot \mu m^{-1}$); DN^i is the digital number of band i; G^i is the gain of THEOS for band i ($Wm^{-2}\cdot sr^{-1}\cdot \mu m^{-1}$) as shown in Table 3.

Table 3. THEOS spectral ranges, gain numbers, and mean exo-atmospheric solar irradiances ($ESUN^i_\lambda$) for cassava and sugarcane.

Spectral Range		***Gain:** $Wm^{-2}\cdot sr^{-1}\cdot\mu m^{-1}$			** $ESUN^i_\lambda$
(nm)	**Gain Number**	**Cassava**	**Gain Number**	**Sugarcane**	$Wm^{-2}\cdot sr^{-1}\cdot\mu m^{-1}$
450-520	G6	2.937	G4	1.468	1983
530-600	G5	2.122	G4	1.501	1813
620-690	G6	3.420	G4	1.710	1552
770-900	G4	1.671	G4	1.671	962

* THEOS image header files; ** Thuillier solar spectrum [24].

The spectral radiance at a sensor's aperture for each band of Landsat 5 TM was calculated using the following equation [22]:

$$L^i{}_{\lambda_{Landsat\,5\,TM}} = \left(\frac{L^i{}_{MAX} - L^i{}_{MIN}}{DN^i{}_{MAX} - DN^i{}_{MIN}} \right) \times \left(DN^i - DN^i{}_{MIN} \right) + L^i{}_{MIN} \quad (2)$$

where $L^i{}_{\lambda_{Landsat\,5\,TM}}$ is the spectral radiance at a sensor's aperture for Landsat 5 TM ($Wm^{-2}\cdot sr^{-1}\cdot\mu m^{-1}$); DN^i is the digital number of band i; $DN^i{}_{MAX}$ and $DN^i{}_{MIN}$ are the maximum (255) and minimum (1) digital number of band i; $L^i{}_{MAX}$ and $L^i{}_{MIN}$ ($Wm^{-2}\cdot sr^{-1}\cdot\mu m^{-1}$) are the spectral radiances at the sensor's aperture scaled to $DN^i{}_{MAX}$ and $DN^i{}_{MIN}$, which were stored in the header file of Landsat 5 TM [22]. The values of $L^i{}_{MAX}$ and $L^i{}_{MIN}$ used in this study are shown in Table 4.

Table 4. Landsat 5 TM spectral ranges, gains ($L^i{}_{MAX}$ and $L^i{}_{MIN}$), and mean exo-atmospheric solar irradiances ($ESUN^i_\lambda$) for cassava and sugarcane.

Landsat 5 TM (LPGS) ($DN^i{}_{MIN}$ =1 and $DN^i{}_{MAX}$ =255)			
Spectral Range (nm)	***Gain:** $Wm^{-2}\cdot sr^{-1}\cdot\mu m^{-1}$		** $ESUN^i_\lambda$
	$L^i{}_{MIN}$	$L^i{}_{MAX}$	$Wm^{-2}\cdot sr^{-1}\cdot\mu m^{-1}$
450-520	−1.52	193	1,983
520-600	−2.84	365	1,796
630-690	−1.17	264	1,536
760-900	−1.51	221	1,031

* Landsat 5 TM image header files; ** Thuillier solar spectrum [24].

The second step of the atmospheric correction involved the conversion of spectral radiance at the sensor's aperture (L_λ) into the exo-atmospheric top-of-the-atmosphere (TOA) reflectance (ρ_{TOA}). This process reduces the scene-to-scene variability, also known as the in-band planetary albedo. The exo-atmospheric TOA reflectance of the earth was computed based on the following equation [22]:

$$\rho^i{}_{TOA} = \frac{\pi * L^i{}_\lambda * d^2}{ESUN^i{}_\lambda * \cos(\theta_s)} \quad (3)$$

where $\rho^i{}_{TOA}$ is the TOA reflectance (unitless); $L^i{}_\lambda$ is the spectral radiance at the sensor's aperture ($Wm^{-2}\cdot sr^{-1}\cdot\mu m^{-1}$); d is Earth-Sun distance (astronomical units); $ESUN^i{}_\lambda$ is the mean exo-atmospheric solar irradiance ($Wm^{-2}\cdot sr^{-1}\cdot\mu m^{-1}$); θ_s is the solar zenith angle (rad) or the value of the sine function of the solar elevation angle.

Calculation of the TOA reflectance requires the exo-atmospheric solar irradiance ($ESUN^i_\lambda$), the Earth–Sun distance (d), and the solar zenith angle (θ_s), which are stored in the header files of THEOS and Landsat 5 TM. Tables 3 and 4 summarize the exo-atmospheric solar irradiances ($ESUN^i_\lambda$) for the THEOS and Landsat 5 TM sensors using the Thuillier solar spectrum [24]. Table 5 presents d in astronomical units throughout a one-year period and the values of θ_s.

Table 5. Acquisition dates, times, Earth-Sun distances (d), and sun and view geometrics (θ: zenith angle and $\emptyset$: azimuth angle).

Sensor	*Date (dd/mm/yy)	*Time UTC	**Earth-Sun distance (d)	*θ_{sun} (deg)	*$\emptyset_{sun}$ (deg)	*θ_{view} (deg)	*$\emptyset_{view}$ (deg)
THEOS	29/11/08	3h13	0.9727	44.30	143.50	34.92	177.57
	9/02/09	3h29	0.9734	43.22	132.65	13.86	199.57
Landsat 5 TM	11/12/08	3h15	0.9693	45.79	144.29	0.07	357.06
	11/02/09	3h29	0.9680	42.41	130.57	0.08	357.06

* THEOS and Landsat 5 TM image header files; ** Chander *et al*. [22].

Finally, in the last step of atmospheric correction, the exo-atmospheric TOA reflectance (ρ_{TOA}) was converted into surface reflectance (ρ_λ). The atmospheric code of the Second Simulation of the Satellite Signal in the Solar Spectrum (6S) model was selected for converting the exo-atmospheric TOA reflectance into surface reflectance. The input parameters of 6S include: (1) geometric conditions; (2) an atmospheric model for gaseous components; (3) an aerosol model (type and concentration); (4) spectral conditions; and (5) field reflectance (type and spectral variation). Based on the above mentioned input parameters, three atmospheric correction coefficients for each band were obtained from the 6S model. Moreover, the atmospheric code for 6S predicts the satellite signal between 0.25 and 4.0 μm, and assumes a cloudless atmosphere taking into account the main atmospheric effects of the absorption by water vapor, carbon dioxide, oxygen, and ozone, and the scattering by molecules and aerosols [25]. However, there was a limit to the use of 6S in this study because THEOS is a new sensor that is still not defined in the 6S code. Therefore, in this study, the 6S code was applied to THEOS by defining the spectral responses of the THEOS sensors as shown in Figure 3 [11]. The 6S modification is included in the Appendix. Following the 6S model, three coefficients were used for obtaining surface reflectance using the following equation:

$$\rho_\lambda^{\ i} = \frac{xa^i * L^i_\lambda - xb^i}{1 + xc^i (xa^i * L^i_\lambda - xb^i)} \tag{4}$$

where $\rho_\lambda^{\ i}$ is the surface reflectance of band i; L^i_λ is the measured radiance of band i; xa^i, xb^i and xc^i are three coefficients obtained from 6S model.

Figure 3. Spectral responses of the THEOS and Landsat 5 TM multi-spectral sensors Source: Geo-Informatics and Space Technology Development Agency (Public Organization) [11]; European Space Agency (ESA) [26].

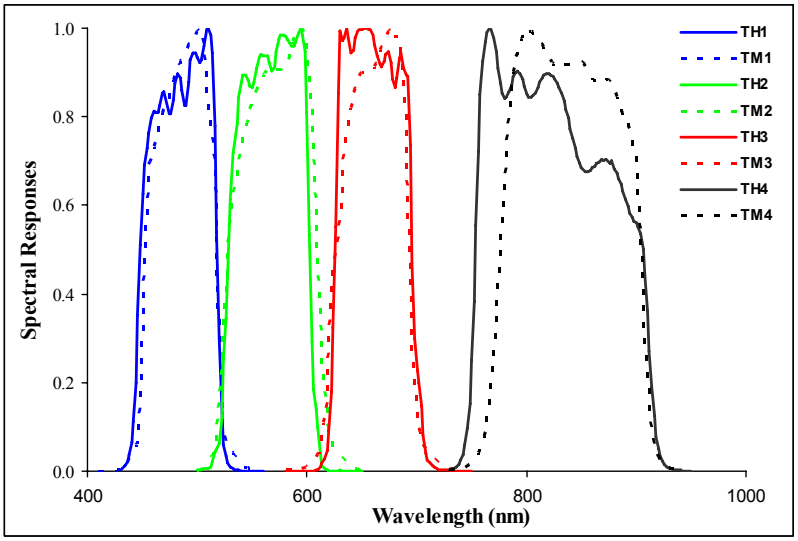

3.3. Regressions Analysis and NDVI Computation

Empirical relationships between the surface reflectance in the visible/near-infrared bands and NDVI were developed and analysed for all sensors. Models were evaluated using coefficients of determination (R^2) and root mean square errors (RMSE). The NDVI computation typically uses surface reflectance in the red and near-infrared bands (Equation (5)) for Landsat 5 TM, and THEOS sensors:

$$\text{NDVI} = \frac{NIR - R}{NIR + R} \tag{5}$$

where NIR is the surface reflectance in the near-infrared band, and R is the surface reflectance in the red band.

The relationship between THEOS (high-resolution) measurements of vegetation and more frequent measurements of Landsat 5 TM (lower-resolution) systems were considered. The regression analysis relating the NDVI of THEOS and Landsat 5 TM was conducted using their original pixel sizes (15 m resolution for THEOS and 30 m resolution for Landsat 5 TM) and the re-sampled pixel sizes of THEOS (from 15 m resolution to 30 m resolution) and Landsat 5 TM (from 30 m resolution to 15 m resolution).

3.4. Classification and Accuracy Assessment

The most widely adopted parametric classification algorithm is the maximum likelihood classifier (MLC) method [27–30]. This method was employed to classify the satellite images. Fifty training points for each class were used for image classification. The existing knowledge of land use was identified by the land use map for MY 2008/09. The THEOS and Landsat 5 TM satellite images (Figure 2(a,b)) for Nakhon Ratchasima Province (cassava site) were classified into six classes: water, forest, paddy field, sugarcane, and cassava. The satellite images (Figure 2(c,d)) for Suphanburi

province (sugarcane site) were classified into four classes: water, forest, bare land, and sugarcane. The accuracy assessment of map classification was identified by the overall accuracy, the user's and producer's accuracies, and the Kappa statistics, which are given in the form of an error matrix that can be used to derive a series of descriptive and analytical statistics [31,32].

4. Results and Discussions

The inter-sensor relationships are presented and discussed based on the data from the two study areas (Figure 1(a,b)). The presents of spectral characteristics of the biofuel crops, a comparison of THEOS and Landsat 5 TM, Inter-sensor NDVI regression analysis for multiple satellite sensors, and classification and accuracy assessment are presented in the following subsections:

4.1. Spectral Characteristics of Biofuel Crops

The spectral characteristics of the two biofuel crops are plotted using the mean of the percent surface reflectance of the samples at the center wavelength of the visible and near-infrared bands of the THEOS and Landsat 5 TM satellite images (Table 2). The surface reflectance of the biofuel crops, based on the satellite sensors, is normalized to surface reflectance using the 6S model. Normalization is necessary to account for the variations in sensor degradation, sun angle, and a host of other calibration factors listed in Tables 1–5.

Figure 4. Mean of the percent surface reflectance in the blue, green, red and near-infrared bands of THEOS and Landsat 5 TM for cassava and sugarcane.

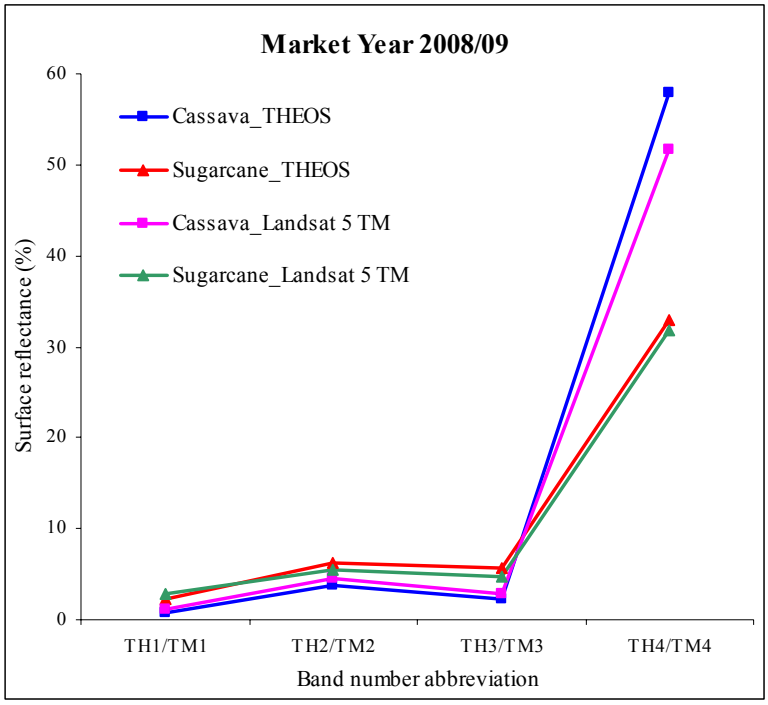

The results show that the spectral characteristics of cassava and sugarcane were similar for both sensors (Figure 4). Specifically, the reflectance was low in the visible region (THEOS: TH1, TH2, and TH3 bands; Landsat 5 TM: TM1, TM2, and TM3 bands), but high in the near-infrared (THEOS: TH4

band; Landsat 5 TM: TM4 band). The results are indicative of the spectral reflectance of vegetation that absorbs in the visible wavelengths (500–750 nm) and has reflectance in the near-infrared at 750–1,350 nm [33]. However, there was a minor difference in surface reflectance in the visible wavelength and a significant difference in the near-infrared wavelength between the two crops as indicated in Figure 4. The noticeable difference in the surface reflectance of the near-infrared wavelength is useful for distinguishing the two types of biofuel crops. The difference between cassava and sugarcane in the surface reflectance of the near-infrared band of THEOS (~28%) was higher than that of Landsat 5 TM (~20%). As a consequence, THEOS can discriminate between cassava and sugarcane better than Landsat 5 TM because the spatial resolution of THEOS is higher than that of Landsat 5 TM.

4.2. Comparison of Landsat 5 TM and THEOS

Sixty surface reflectance samples were used to compare THEOS and Landsat 5 TM (Figure 1(a,b)) results for the visible/near-infrared bands and NDVI of the two biofuel crop fields. Relationships between the THEOS and Landsat 5 TM surface reflectances for the visible/near-infrared bands and NDVI of the two biofuel crops were also established (Table 6 and Figure 5).

The results indicated a strong relationship and positive association, where higher visible/near-infrared and NDVI of THEOS correspond to higher visible/near-infrared and NDVI of Landsat 5 TM and lower visible/near-infrared and NDVI of THEOS correspond to lower visible/near-infrared and NDVI of Landsat 5 TM. Furthermore, the RMSE was also small significant difference between the visible/near-infrared and NDVI of THEOS and Landsat 5 TM in cassava and sugarcane.

Figure 5. Relationships between THEOS and Landsat 5 TM surface reflectances for two biofuel crops. (**a**) Blue. (**b**) Green. (**c**) Red. (**d**) Near-infrared (NIR) bands. (**e**) NDVI.

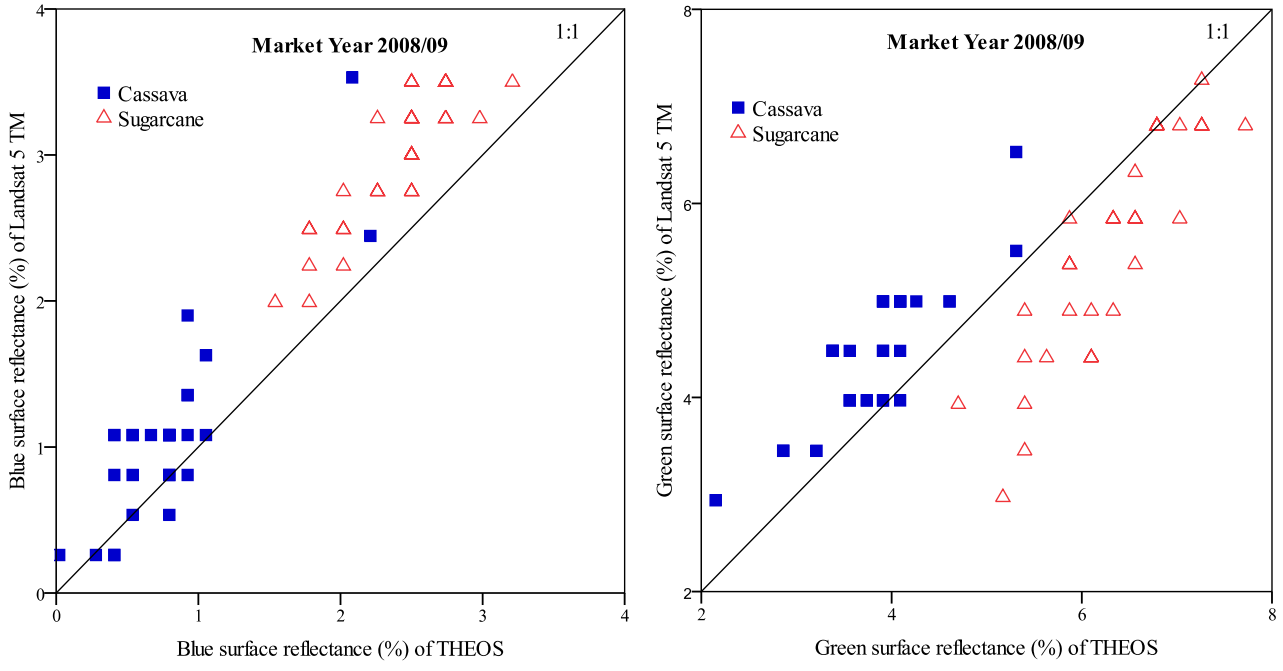

(**a**) (**b**)

Figure 5. *Cont.*

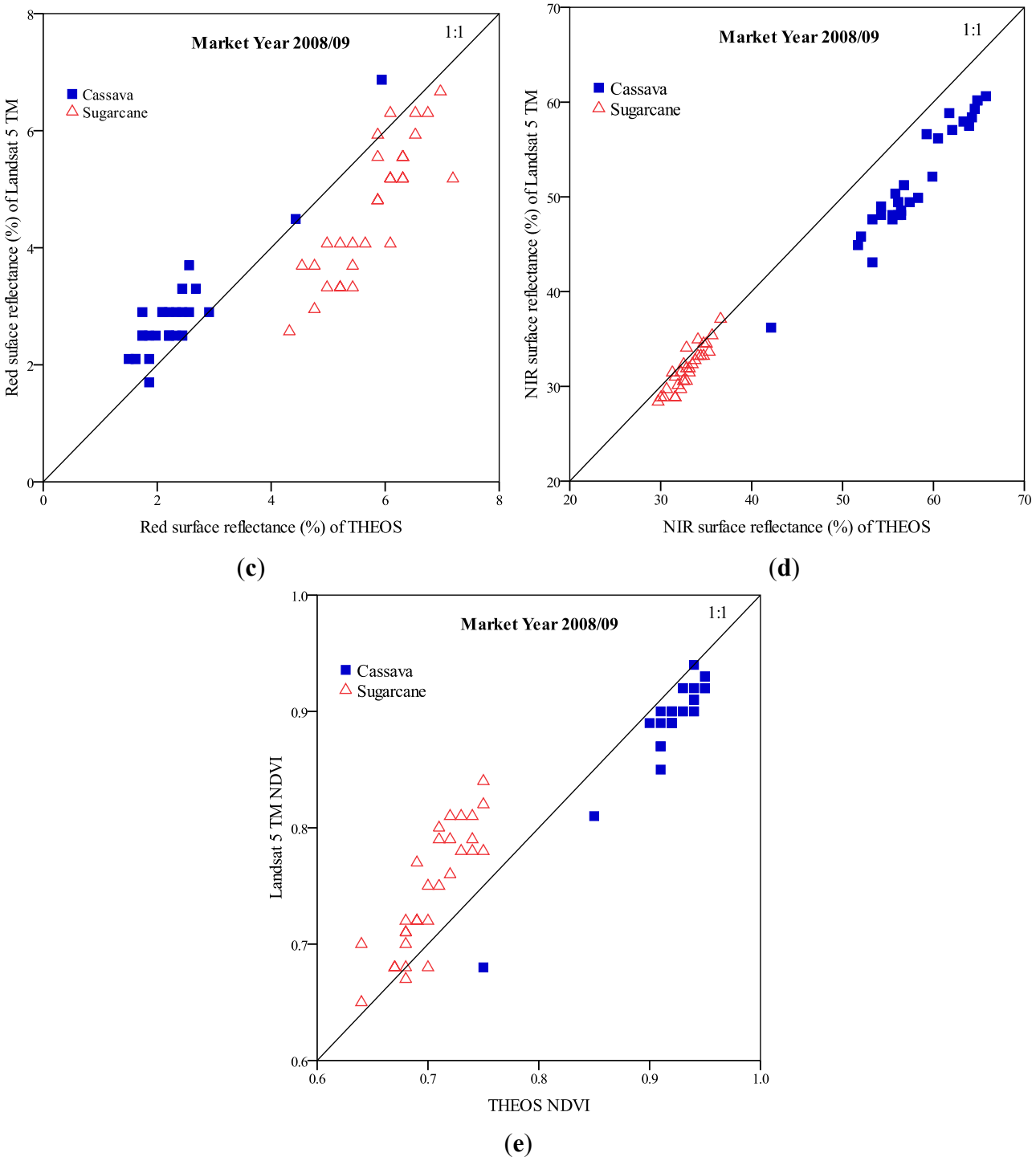

The results indicate that there is a strong relationship between THEOS and Landsat 5 TM surface reflectances of the visible/near-infrared bands and the NDVI of the two biofuel crops and that the results are similar to other inter-sensor studies on vegetation [6,8]. Therefore, THEOS has a radiometric capability that corresponds with Landsat 5 TM for both cassava and sugarcane. Theoretically, the results should be verified for accuracy ground truth spectra along with the acquisition of images. However, because of the lack of ground truth spectra, Landsat 5 TM was used instead.

Table 6. Statistics linear regressions between THEOS and Landsat 5 TM surface reflectances for cassava and sugarcane (95% confidence level).

Band	Cassava		Sugarcane	
	R^2	RMSE	R^2	RMSE
TH1	0.75	0.46	0.76	0.61
TH2	0.73	0.73	0.77	1.01
TH3	0.87	0.60	0.73	1.27
TH4	0.93	6.42	0.82	1.44
NDVI	0.94	0.03	0.74	0.04

4.3. Inter-Sensor NDVI Regression Analysis for Multiple Satellite Sensor Applications

These results indicated that the relationships between the THEOS and Landsat 5 TM for NDVI data for cassava and sugarcane had strong relationships as illustrated in the training data column of Table 7. The R^2 obtained from the transformation of the lower spatial resolution to the higher spatial resolution were higher than that of the opposite transformation, but the RMSE trend is the reverse. Finally, the relationships of NDVI at the THEOS resolution (15 m) were better than at the Landsat 5 TM resolution (30 m).

Table 7. Statistics linear regressions between THEOS and Landsat 5 TM at 15 and 30 m resolution for NDVI for cassava and sugarcane.

THEOS *vs.* Landsat 5 TM (15 m)	**Training Data**		**Testing Data**	
	R^2	RMSE	R^2	RMSE
Cassava	0.94	0.03	0.88	0.01
Sugarcane	0.74	0.04	0.73	0.04
Landsat 5 TM *vs.* THEOS (30 m)	**Training Data**		**Testing Data**	
	R^2	RMSE	R^2	RMSE
Cassava	0.70	0.05	0.89	0.06
Sugarcane	0.62	0.14	0.73	0.10

The intercept (a) and slope (b) coefficients (Table 8) can be used to convert the NDVI in one spatial resolution ($NDVI_{Dependent}$) into NDVI in another spatial resolution ($NDVI_{Independent}$) using Equation (6). These results can help in combining data from both THEOS and Landsat 5 TM in case that data from one of them is not available due to various reasons. However, the regression coefficients obtained from such a generalization of inter-sensor relationship would vary, most likely, field-by-field, and even time-to-time.

$$NDVI_{Dependent} = a + b * NDVI_{Independent} \quad (6)$$

For example, the values of Landsat 5 TM at 30 m resolution were re-sampled to THEOS 15 m resolution for cassava. Thus, the calculation is based on Equation (7):

$$\mathrm{NDVI}_{\mathrm{THEOS}} = 0.2338 + 0.7691 * NDVI_{Landsat\,5TM} \quad (7)$$

where the THEOS and Landsat 5 TM subscripts denote sensor derived values for the THEOS and Landsat 5 TM sensors, respectively.

The intercepts (a) and slopes (b) in Table 8 were validated using actual NDVI data for Landsat 5 TM and THEOS for cassava and sugarcane. The actual data was selected for testing data from the two study areas. The predicted NDVI from Landsat 5 TM and THEOS were computed using the intercept (a) and slope (b) coefficients from Table 8 instead of equations (6) for the same testing data for cassava and sugarcane.

Table 8. NDVI intercept (**a**) and slope (**b**) coefficients for THEOS and Landsat 5 TM satellite sensors relationships for cassava and sugarcane.

$NDVI_{Dependent}$	$NDVI_{Independent}$			
	Cassava		Sugarcane	
	THEOS 30 m	Landsat 5 TM 15 m	THEOS 30 m	Landsat 5 TM 15 m
THEOS 15 m	-	a = 0.2338 b = 0.7691	-	a = 0.3417 b = 0.4833
Landsat 5 TM 30 m	a = 0.249 b = 0.752	-	a = 0.109 b = 1.038	

The results indicate the R^2 and RMSE testing data were not different from those of the training data (Table 7). All of the R^2 indicate strong relationships, and the RMSE were very small. The evaluations depicting actual *versus* predicted NDVI values of Landsat 5 TM and THEOS have a high degree of reliability.

4.4. Classification and Accuracy Assessment

The spatial resolution capabilities of THEOS (15 m) and Landsat 5 TM (30 m) for landuse/landcover (LULC) mapping were compared in MY 2008/09. A classification accuracy assessment was performed for the MLC classified maps of THEOS and Landsat 5 TM at the different spatial resolutions of 15 m and 30 m, respectively (Figure 6). The LULC classification accuracy of THEOS at Nakhon Ratchasima Province (Cassava site) was 96% overall accuracy with a kappa coefficient of 0.95, while 93% accuracy and a 0.90 kappa coefficient was achieved by Landsat 5 TM (Tables 9 and 10). The LULC classification accuracy of THEOS at Suphanburi Province (sugarcane site) was 99% overall accuracy with a 0.99 kappa coefficient, while 96% overall accuracy and a 0.92 kappa coefficient was achieved using Landsat 5 TM (Tables 11 and 12). The results show that the THEOS images were capable of classifying and mapping the LULC with a higher overall accuracy and kappa coefficient than the Landsat 5 TM images.

Table 9. Error matrix of landuse/landcover (LULC) classification accuracy assessment for THEOS images of Nakhon Ratchasima Province (Cassava site).

		Reference Data					
		Water	**Forest**	**Paddy field**	**Sugarcane**	**Cassava**	**Total**
Map Data	**Water**	**2,566**	0	6	21	21	2,614
	Forest	0	**3,415**	0	7	177	3,599
	Paddy field	44	0	**8,503**	29	28	8,604
	Sugarcane	489	9	156	**2,015**	548	1,572
	Cassava	39	25	4	18	**29,859**	29,945
	Total	3,138	3,449	8,669	2,090	30,733	47,979

Overall Accuracy = 96% and Kappa Coefficient = 0.95

Producer's Accuracy		User's Accuracy	
Water	= 82%	Water	= 98%
Forest	= 99%	Forest	= 95%
Paddy field	= 98%	Paddy field	= 99%
Sugarcane	= 96%	Sugarcane	= 63%
Cassava	= 98%	Cassava	= 99%

Table 10. Error matrix of LULC classification accuracy assessment for Landsat 5 TM images of Nakhon Ratchasima Province (Cassava site).

		Reference Data					
		Water	**Forest**	**Paddy field**	**Sugarcane**	**Cassava**	**Total**
Map Data	**Water**	**925**	0	2	2	44	973
	Forest	0	**1,242**	0	6	136	1,384
	Paddy field	0	0	**3,148**	2	9	3,159
	Sugarcane	180	20	3	**697**	672	1,572
	Cassava	23	3	22	29	**10,247**	10,324
	Total	3,138	3,449	8,669	2,090	30,733	47,979

Overall Accuracy = 93% and Kappa Coefficient = 0.90

Producer's Accuracy		User's Accuracy	
Water	= 82%	Water	= 95%
Forest	= 98%	Forest	= 90%
Paddy field	= 99%	Paddy field	= 99%
Sugarcane	= 95%	Sugarcane	= 44%
Cassava	= 94%	Cassava	= 98%

Table 11. Error matrix of LULC classification accuracy assessment for THEOS images of Suphanburi Province (sugarcane site).

		Reference Data				
		Water	**Forest**	**Bare land**	**Sugarcane**	**Total**
Map Data	**Water**	**1,336**	0	5	1	1,342
	Forest	2	**560**	22	47	631
	Bare land	29	0	**10,253**	34	10,316
	Sugarcane	0	0	43	**16,419**	16,462
	Total	1,367	560	10,323	16,501	28,751

Overall Accuracy = 99% and Kappa Coefficient = 0.99

Producer's Accuracy		User's Accuracy	
Water	= 98%	Water	= 100%
Forest	= 100%	Forest	= 89%
Bare land	= 99%	Bare land	= 100%
Sugarcane	= 100%	Sugarcane	= 99%

Table 12. Error matrix of LULC classification accuracy assessment for Landsat 5 TM images of Suphanburi Province (sugarcane site).

		Reference Data				
		Water	**Forest**	**Bare land**	**Sugarcane**	**Total**
Map Data	**Water**	**484**	0	0	160	644
	Forest	8	**192**	33	171	404
	Bare land	9	0	**3,691**	45	3,745
	Sugarcane	2	14	22	**5,604**	5,642
	Total	530	206	3,746	5,980	10,435

Overall Accuracy = 96% and Kappa Coefficient = 0.92

Producer's Accuracy		User's Accuracy	
Water	= 96%	Water	= 75%
Forest	= 93%	Forest	= 48%
Bare land	= 97%	Bare land	= 99%
Sugarcane	= 94%	Sugarcane	= 99%

Figure 6. The LULC mapping of Nakhon Ratchasima Province (cassava site). (**a**) THEOS. (**b**) Landsat 5 TM and Suphanburi Province (sugarcane site). (**c**) THEOS. (**d**) Landsat 5 TM.

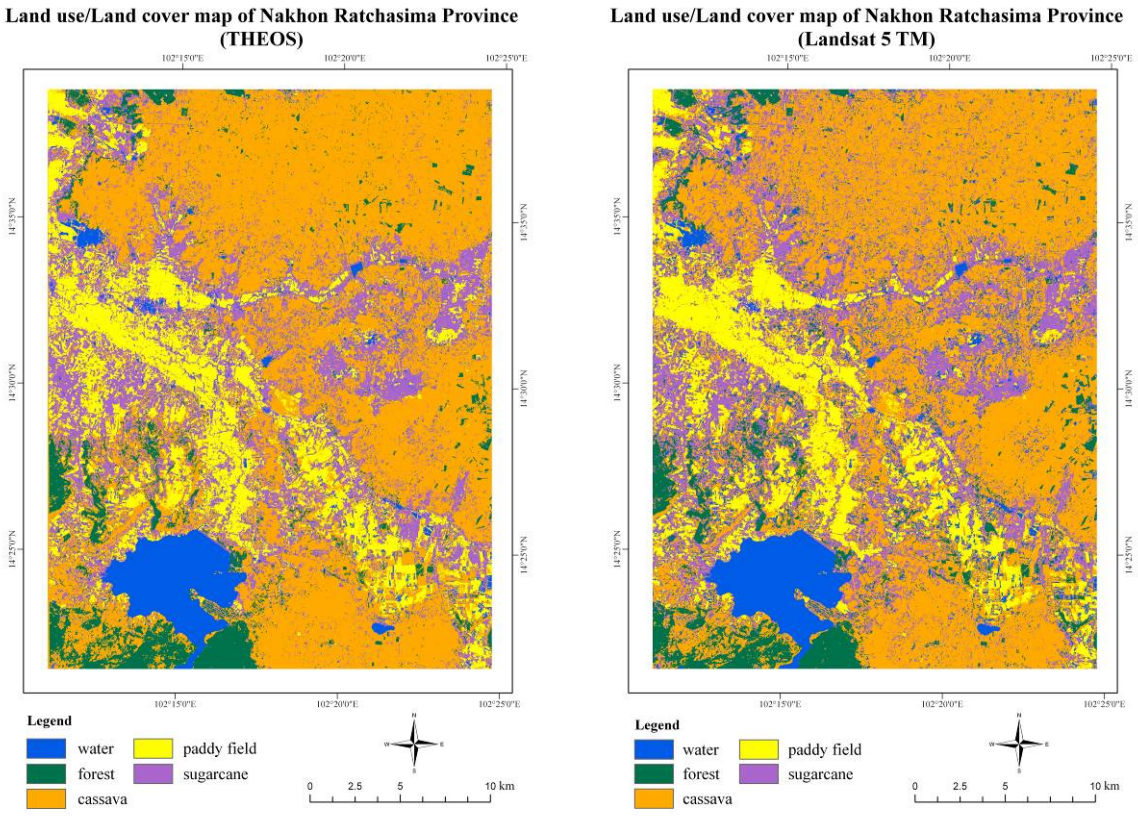

Figure 6. *Cont.*

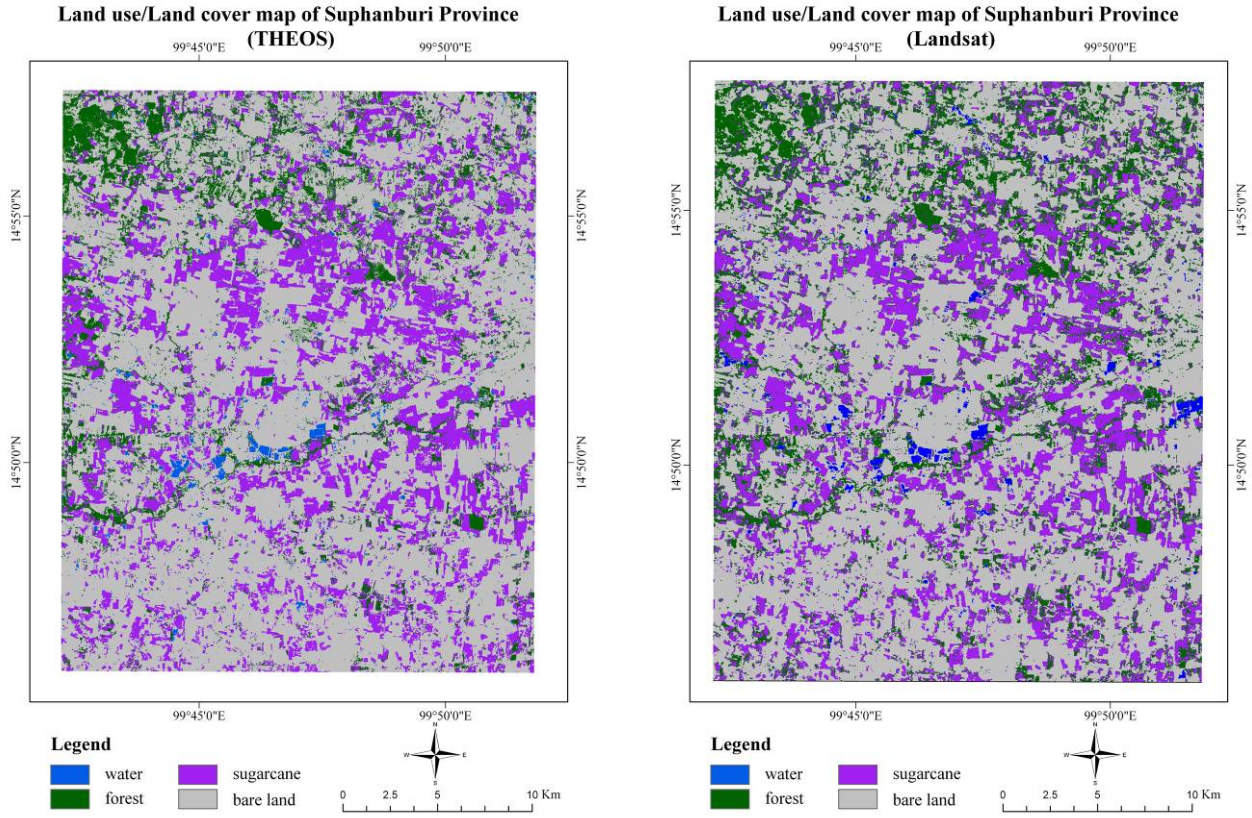

(c) **(d)**

5. Conclusions

The paper presents an inter-sensor comparison of Landsat 5 TM and THEOS for surface reflectance, NDVI including classification for cassava and sugarcane at various study sites in Thailand. It was confirmed that THEOS and Landsat 5 TM are strongly correlated and can serve to be an alternate data source to each other in case data from one is not available. The outcome of the study has established that:

(a) The spectral characteristics of cassava and sugarcane were quite similar respectively from both sensors specifically in the visible wavelength. However, higher values were found in the near-infrared between the two crops where THEOS could offer slightly better discrimination between cassava and sugarcane than Landsat 5 TM.

(b) Significant strong relationships were obtained between THEOS and Landsat 5 TM surface reflectance and NDVI for cassava and sugarcane.

(c) The regression models to calculate NDVI from one satellite can be used for another. But the model from Landsat 5 TM to THEOS offered poorer R^2. These variations may be due to different spatial resolution and also difference in image acquisition day.

(d) Performance of THEOS and Landsat 5 TM in classifying land cover classes was quite similar. THEOS performed slightly better, but not really much of a difference. This may be due to original resolution of Theos is 15 m as compared to 30 m of Landsat 5 TM.

This study found that the differences in sensor degradations, especially regarding TM5 which has been operated far longer than its expected lifespan, may largely influence classification accuracies.

Since the original spatial resolution is different between the two sensors, there must be a fundamental difference even though this study conducted precise co-registration and re-sampling. This fundamental difference may influence the accuracies both in cross-calibration and classification. Moreover, the regression results may be different if one uses much coarser spatial resolution, since by doing so we expect much less influence from geometric accuracy.

Further studies are needed for other crops and landuse/landcover types for inter-sensor calibrations of radiometric, spatial, and temporal characteristics to overcome problems of data limitation due to cloud cover and revisit periods.

Acknowledgements

Assistance received from the Geo-Informatics and Space Technology Development Agency (Public Organization) in acquiring the THEOS and Landsat 5 TM satellite imagery is gratefully acknowledged. Comments received from Laor Boongasame and Rujee Rodcha is sincerely appreciated. This research is funded by the Agricultural Research Development Agency (Public Organization), Thailand.

References

1. Strengers, B.; Leemans, R.; Eickhout, B.; de Vries, B.; Bouwman, L. The land-use projections and resulting emissions in the IPCC SRES scenarios as simulated by the IMAGE 2.2 model. *GeoJournal* **2004**, *61*, 381-393.
2. Smeets, E.M.W.; Faaij, A.P.C.; Lewandowski, I.M.; Turkenburg, W.C. A bottom-up assessment and review of global bio-energy potentials to 2050. *Prog. Energ. Combust.* **2007**, *33*, 56-106.
3. Hellmann, F.; Verburg, P.H. Spatially explicit modelling of biofuel crops in Europe. *Biomass Bioenerg.* **2008**, *35*, 2411-2424.
4. Plummer, S.E. Perspectives on combining ecological process models and remotely sensed data. *Ecol. Model.* **2000**, *129*, 169-186.
5. Soudani, K.; François, C.; Maire, G.; Dantec, V.; Dufrêne, E. Comparative analysis of IKONOS, SPOT, and ETM+ data for leaf area index estimation in temperate coniferous and deciduous forest stands. *Remote Sens. Environ.* **2003**, *102*, 161-175.
6. Hill, J.; Aifadopoulou, D. Comparative analysis of Landsat-5 TM and SPOT HRV-1 data for use in multiple sensor approaches. *Remote Sens. Environ.* **1990**, *34*, 55-70.
7. Dinguirard, M.; Slater, N.P. Calibration of space-multispectral imaging sensors: A review. *Remote Sens. Environ.* **1999**, *68*, 194-205.
8. Steven, D.M.; Malthus, J.T.; Baret, F.; Xu, H.; Chopping, J.M. Intercalibration of vegetation indices from different sensor systems. *Remote Sens. Environ.* **2003**, *88*, 412-422.
9. Thenkabail, S.P. Inter-sensor relationships between IKONOS and Landsat-7 ETM+ NDVI data in three ecoregions of Africa. *Int. J. Remote Sens.* **2004**, *25*, 389-408.
10. Miura, T.; Yoshioka, H.; Fujiwara, K.; Yamamoto, H. Inter-comparison of ASTER and MODIS surface reflectance and vegetation index products for synergistic applications to natural resource monitoring. *Sensors* **2008**, *8*, 2480-2499.

11. GISTDA. *Thailand Earth Observation System (THEOS)*; Geo-Informatics and Space Technology Development Agency (Public Organization), Ministry of Science and Technology: Bangkok, Thailand, 2009. Available online: http://gistda.or.th (accessed on 9 December 2009).
12. Bricaud, A.; Bosc, E.; Antoine D. Algal biomass and sea surface temperature in the Mediterranean Basin: Intercomparison of data from various satellite sensors, and implications for primary production estimates. *Remote Sens. Environ.* **2002**, *81*, 163-178.
13. Zwiggelaar, R. A review of spectral properties of plants and their potential use for crop/weed discrimination in row-crops. *Crop Prot.* **1998**, *17*, 189-206.
14. Campbell, J.B. *Introduction to Remote Sensing*, 2nd ed.; Taylor & Francis: London, UK, 2002; pp. 461-463.
15. Galvão, L.S.; Formaggio, A.R.; Tisot, D.A. Discrimination of sugarcane varieties in Southeastern Brazil with EO-1 Hyperion data. *Remote Sens. Environ.* **2005**, *94*, 523-534.
16. Xaviera, A.C.; Rudorff, B.F.T.; Shimabukuro, Y.E.; Berka, L.M.S.; Moreira, M.A. Multi-temporal analysis of MODIS data to classify sugarcane crop. *Int. J. Remote Sens.* **2006**, *27*, 755-768.
17. Bell, R.D.; Silalertruksa T.; Gheewala, H.S.; Kamens, R. The net cost of biofuels in Thailand: An economic analysis. *Energy Policy* **2011**, *32*, 834-843.
18. Krukanont, P.; Prasertsan, S. Geographical distribution of biomass and potential sites of rubber wood red power plants in Southern Thailand. *Biomass Bioenerg.* **2004**, *26*, 47-59.
19. Thampanya, U.; Vermaat, J.E.; Sinsakul, S.; Panapitukkul, N. Coastal erosion and mangrove progradation of Southern Thailand. *Estuar. Coast. Shelf Sci.* **2006**, *68*, 75-85.
20. Entwisle, B.; Rindfuss, R.R.; Walsh, S.J.; Page, P.H. Population growth and its spatial distribution as factors in the deforestation of Nang Rong, Thailand. *Geoforum* **2008**, *39*, 879-897.
21. Choowong, M.; Phantuwongraj, S.; Charoentitirat, T.; Chutakositkanon, V.; Yumuang, S.; Charusiri, P. Beach recovery after 2004 Indian Ocean tsunami from Phang-nga, Thailand. *Geomorphology* **2009**, *104*, 134-142.
22. Chander, G.; Markham, B. L.; Helder, D. L. Summary of current radiometric calibration coefficients for Landsat MSS, TM, ETM+, and EO-1 ALI sensors. *Remote Sens. Environ.* **2009**, *113*, 893-903.
23. Rajapakse, R.M.S.S.; Tripathi, N.K.; Honda, K. Spectral characterization and LAI modeling for the tea (Camellia sinensis (L.) O. Kuntze) canopy. *Int. J. Remote Sens.* **2002**, *23*, 3569-3577.
24. Thuillier, G.; Herse, M.; Labs, S.; Foujols, T.; Peetermans, W.; Gillotay, D.; Simon, P.C.; Mandel, H. The solar spectral irradiance from 200 to 2400 nm as measured by SOLSPEC Spectrometer from the ATLAS 123 and EURECA missions. *Solar Physics* **2003**, *214*, 1-22.
25. Vermote, E.F.; Tanre, D.; Deuze, J.L.; Herman, M.; Morcrette, J.J. Second simulation of the satellite signal in the solar spectrum, 6S: An overview. *IEEE Trans. Geosci. Remote Sens.* **1997**, *35*, 675-686.
26. European Space Agency (ESA). *Spectral Response Function Information of Landsat 5 TM*; Available online: http://calvalportal.ceos.org/cvp/web/guest/landsat-5-tm (accessed on 9 December 2009)
27. Liu, X.H.; Skidmore, A.K.; Oosten, H.V. Integration of classification methods for improvement of land cover map accuracy. *ISPRS J. Photogramm.* **2002**, *56*, 257-268.

28. Currit, N. Development of remotely sensed, historical land cover change database for rural Chihuahua, Mexico. *Int. J. Appl. Earth Obs. Geoinf.* **2005**, *7*, 232-247.
29. Bailly, J.S.; Arnaud, M.; Puech, C. Boosting: A classification method for remote sensing. *Int. J. Remote Sens.* **2007**, *28*, 1687-1710.
30. Ramita, M.; Inakwu, O.A.O.; Tiho, A. Improving the accuracy of land use and land cover classification of Landsat data using post-classification enhancement. *Remote Sens.* **2009**, *1*, 330-344.
31. Congalton, R.G. A review of assessing the accuracy of classification of remotely sensed data. *Remote Sens. Environ.* **1991**, *37*, 35-46.
32. Congalton, R.G.; Green, K. *Assessing the Accuracy of Remotely Sensed data: Principles and Practices*, 2nd ed.; CRC Press: Boca Raton, FL, USA, 2009; p. 183.
33. Colwell, R.N. *Manual of Remote Sensing*, 2nd ed.; American Society of Photogrammetry: Falls Church, VA, USA, 2002; Volume II, p. 2138.

Appendix

The 6S code (Version 4.1) was applied to THEOS by defining the spectral responses of the THEOS sensors. The spectral response is provided by a step of 0.0025 micrometer (μm) as shown in 6S new subroutines.

6S Main

```
program ssssss
data etiq1/
s '(1h*,22x,34h user defined conditions ,t79,1h*)',
s ' theos 1 ',' theos 2 ',
s ' theos 3 ',' theos 4 ',

c*************************************************************************c
c iwave input of the spectral conditions c
c ------------------------------- c
c 61 THEOS band 1 (0.450-0.520) c!RS140507
c 62 THEOS band 2 (0.530-0.600) c!RS140507
c 63 THEOS band 3 (0.620-0.690) c!RS140507
c 64 THEOS band 4 (0.770-0.900) c!RS140507
c note: wl has to be in micrometer c
c*************************************************************************c
do 38 l=iinf,isup
c 132 THEOS band (61,64)!RS140507
 18 goto (110,111,112,112,114,114,114,114,114,114,114,114
 s ,114,114,114,114,118,118,118,118,118,118,118,118
 s ,121,121,121,121,121,121,127,127,127,127
 s ,128,128,128,128,128,128,128,129,129,129,129,129
 s ,129,129,130,130,130,130
```

```
 s ,131,131,131,131,131,131,131,131,132,132,132,132),iwave
 110 read(iread,*) wlinf,wlsup
 132 call theos(iwave-60)
      19 iinf=(wlinf-.25)/0.0025.5
       isup=(wlsup-.25)/0.0025.5
      20 continue
```

6S New Subroutines:

```
 subroutine theos (iwa)
 real s,wlinf,wlsup
 common /sixs_ffu/ s(1501),wlinf,wlsup
 real sr(4,1501),wli(4),wls(4)
 integer iwa,l,i

c 1st spectral band of THEOS (multi-spectral)

 data (sr(1,l),l=1,1501)/72*0.,
 a 0.0045, 0.0083, 0.0163, 0.0322, 0.0658, 0.1340, 0.2759, 0.6278,
 a 0.6258, 0.6997, 0.7461, 0.7889, 0.8122, 0.8100, 0.8178, 0.8462,
 a 0.8571, 0.8262, 0.8079, 0.8297, 0.8767, 0.8959, 0.8744, 0.8339,
 a 0.8267, 0.8917, 0.9372, 0.9430, 0.9339, 0.9244, 0.9443, 0.9874,
 a 1.0000, 0.9743, 0.8624, 0.5996, 0.3001, 0.1121, 0.0468, 0.0235,
 a 0.0100, 0.0046, 0.0029, 0.0021, 0.0012, 0.0007, 0.0005, 0.0004,
 a 0.0003, 0.0002, 0.0002, 0.0001, 0.0001,
 a 1376*0./
c
c 2nd spectral band of THEOS (multi-spectral)

 data (sr(2,l),l=1,1501)/ 100*0.,
 a 0.0040, 0.0029, 0.0046, 0.0072, 0.0072, 0.0129, 0.0327, 0.0471,
 a 0.0614, 0.1537, 0.2979, 0.4166, 0.6152, 0.1537, 0.2979, 0.4166,
 a 0.6152, 0.7244, 0.7609, 0.8286, 0.8793, 0.8944, 0.8874, 0.8729,
 a 0.8673, 0.8872, 0.9220, 0.9392, 0.9376, 0.9387, 0.9295, 0.9080,
 a 0.9140, 0.9554, 0.9807, 0.9837, 0.9803, 0.9724, 0.9625, 0.9587,
 a 0.9676, 0.9917, 0.9921, 0.9557, 0.8115, 0.4726, 0.2384, 0.1515,
 a 0.0985, 0.0328, 0.0088, 0.0030, 0.0014, 0.0011, 0.0010, 0.0014,
 a 0.0018, 0.0008, 0.0004, 0.0001, 0.0001,
 a 1340*0./
c
c 3rd spectral band of THEOS (multi-spectral)

 data (sr(3,l),l=1,1501)/ 136*0.,
 a 0.0001, 0.0002, 0.0003, 0.0003, 0.0004, 0.0004, 0.0007, 0.0015,
```

```
 a 0.0043, 0.0123, 0.0226, 0.0410, 0.0901, 0.2162, 0.4384, 0.7787,
 a 0.9924, 0.9721, 0.9885, 0.9827, 0.9445, 0.9572, 0.9872, 0.9955,
 a 0.9960, 0.9995, 0.9986, 0.9966, 0.9846, 0.9567, 0.9292, 0.9154,
 a 0.9242, 0.9413, 0.9341, 0.8934, 0.8646, 0.8980, 0.9364, 0.9184,
 a 0.8951, 0.8515, 0.6029, 0.3411, 0.2289, 0.1864, 0.1137, 0.0513,
 a 0.0254, 0.0170, 0.0118, 0.0072, 0.0040, 0.0026, 0.0020, 0.0017,
 a 0.0016, 0.0013, 0.0009, 0.0006, 0.0003, 0.0002, 0.0002, 0.0002,
 a 0.0002,
 a 1300*0./
c
c 4th spectral band of THEOS (multi-spectral)

 data (sr(4,l),l=1,1501)/192*0.,
 a 0.0040, 0.0058, 0.0089, 0.0144, 0.0239, 0.0426, 0.0771, 0.1394,
 a 0.2485, 0.4261, 0.6373, 0.8178, 0.9259, 0.9736, 0.9948, 0.9979,
 a 0.9783, 0.9377, 0.8928, 0.8580, 0.8402, 0.8466, 0.8644, 0.8853,
 a 0.9005, 0.9029, 0.8914, 0.8741, 0.8520, 0.8443, 0.8426, 0.8487,
 a 0.8655, 0.8802, 0.8907, 0.8962, 0.8959, 0.8933, 0.8875, 0.8778,
 a 0.8656, 0.8489, 0.8264, 0.8018, 0.7738, 0.7451, 0.7199, 0.6983,
 a 0.6838, 0.6772, 0.6759, 0.6776, 0.6852, 0.6870, 0.6911, 0.6987,
 a 0.7008, 0.7027, 0.6972, 0.6990, 0.6831, 0.6706, 0.6541, 0.6350,
 a 0.6144, 0.5937, 0.5775, 0.5668, 0.5600, 0.5481, 0.5187, 0.4568,
 a 0.3626, 0.2515, 0.1576, 0.0908, 0.0510, 0.0299, 0.0178, 0.0109,
 a 0.0068, 0.0046, 0.0035, 0.0024, 0.0016, 0.0012, 0.0009, 0.0007,
 a 0.0005,
 a 1220*0./

 wli(1)=0.43
 wls(1)=0.56
 wli(2)=0.5
 wls(2)=0.65
 wli(3)=0.59
 wls(3)=0.75
 wli(4)=0.73
 wls(4)=0.95
 do 1 i=1,1501
 s(i)=sr(iwa,i)
 1 continue
 wlinf=wli(iwa)
 wlsup=wls(iwa)
 return
 end
```

Sensor Required Information to Run 6S

The 6S option used "0 ": "user condition". The 6S required pieces of information are: the solar zenith angle (SZA), the solar azimuth angle (SAZ), the view zenith angle (VZA) and the view azimuth angle (VAZ).

****

Input of band blue for sugarcane

0	//user condition
43.22 132.65 13.86 199.58 02 09	//SZA, SAZ, VZA, VAZ, month, day
1	// Tropical
1	//Continental
10	//visibility (10 km)
−0.062	//−altitude (0.062 km)
−1000	//sensor aboard a satellite
61	//theos Band 1
1	//non homogeneous surface
1 1 0.5	//vegetation target, environment, radius (0.5 km)
−0.0303987	//apparent reflectance RAPP = −ρ(TOA)

****

****

Atmospheric correction result of band blue for sugarcane

* input apparent reflectance : 0.030	*
* measured radiance [w/m2/sr/mic] : 14.200	*
* atmospherically corrected reflectance : −0.131	*
* coefficients xa xb xc : 0.00355 0.18031 0.19496	*
* y = xa*(measured radiance) − xb; acr=y/(1.+ xc*y)	*

****